Hydrothermally Processed TiO_2 Nanowire Electrodes with Antireflective and Electrochromic Properties

Jing-Zhi Chen, Wen-Yin Ko, Yin-Cheng Yen, Po-Hung Chen, and Kuan-Jiuh Lin*

Department of Chemistry, National Chung Hsing University, Taichung 402, Taiwan

ABSTRACT

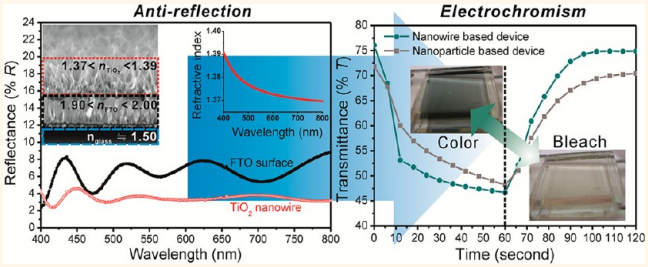

Dual functionalities of antireflective and electrochromic properties-based anatase TiO_2 nanowire devices with a high-porosity cross-linked geometry directly grown onto transparent conductive glass was achieved for the first time through a simple one-step hydrothermal process under mild alkali conditions. Devices fashioned from these TiO_2 nanowires were found to display enhanced optical transparency in the visible range, better color contrast, and faster color-switching time in comparison to devices made from nanoparticles. These improvements can be attributed to the low refractive index and high porosity of the TiO_2 nanowires and their larger accessible surface area for Li^+ intercalation and deintercalation, leading to enhanced capabilities for transparent electrochromic smart windows.

KEYWORDS: TiO_2 nanowire · porous structure · antireflection · transparent device · electrochromism

Smart windows constructed of semiconducting electrochromic materials on conductive glass have been widely used in the energy-saving glass industry.[1,2] However, these smart windows typically exhibit low visible transmittance in the transparent state, reducing their usefulness in some applications. In general, the visible transmittance of electrochromic glass in the transparent state (60−70%) is much lower than that of regular window glass (>80%),[3] delivering a less comfortable visual environment in buildings. Currently, antireflective (AR)-coating technologies have been aimed at improving the light transmittance and visual appearance of smart windows.[3−5] However, this additional AR-coating process is a significant extra expense for fabricating electrochromic glasses. Hence, a great challenge for scientists is to develop a one-step fabricating technique for creating a semiconducting layer with both AR and electrochromic properties.

Chemically stable anatase TiO_2 nanocrystals with tetragonal symmetry, formed from TiO_6 octahedra, is the most promising material currently being used in electrochromism studies because the vacant sites formed by the shared edges are large enough to accommodate H^+ and Li^+ ions.[6,7] Also, anatase TiO_2 nanoparticles (NPs) and nano thin films have been proven to serve well as an AR layer for Si, VO_2, and InP substrates due to their suitable refractive indices of 2.1−2.3.[8−10] However, the refractive index of a TiO_2 AR layer on glass-based substrates should be 1.2−1.4 according to the relationship $n_f = (n_0 n_s)^{1/2}$,[11] where n_f, n_0, and n_s are the refractive indices of the AR layer, air, and the substrate, respectively, and the refractive indices of typical conductive glasses (*i.e.*, fluorine-doped tin oxide (FTO) or Sn-doped indium oxide, tin-doped indium oxide (ITO) glass) are closer to 1.5−2.[12,13] Several different approaches have been attempted to reduce the refractive index of TiO_2. Among these methods, Xi *et al.* reported that the refractive index of a TiO_2 nanorod (NR) layer on aluminum nitride substrates can be controlled in a way that reduces the refractive index from 2.7 to 1.3 by changing the vapor-deposition incident angle using the oblique-angle deposition (OAD) method.[14] This finding indicates that the TiO_2 NR layer, consisting of obliquely standing, porous nanostructures, is the key to effectively reducing the

* Address correspondence to kjlin@dragon.nchu.edu.tw.

Received for review February 22, 2012 and accepted July 2, 2012.

Published online July 02, 2012
10.1021/nn300787r

refractive index itself. However, the development of a TiO_2 nanostructure with these features on transparent glass-based substrates by using the same OAD methods has proven to be a challenge. To the best of our knowledge, no refractive index below 1.5 has been obtained using this method.[15−17] Moreover, OAD methods require a high-vacuum environment and a lengthy deposition time, which is not convenient for large-scale production and a one-step fabricating process.

A low-cost alkali hydrothermal method has been applied to the mass production of one-dimensional (1D) TiO_2 nanostructures on bulk titanium substrates such as NRs,[18] NWs,[19,20] and nanotubes (NTs);[21−23] however, this method has disadvantages in that it often needs rigorous experimental conditions consisting of a high alkali concentration, high temperatures, and long processing times. When growing 1D TiO_2 nanostructures on glass-based substrates, surface damage to the glass is likely to happen under such rigorous reaction conditions. In our previous work, we employed a low-cost, two-step process combined with a subsequent annealing treatment for the preparation of controllable 1D anatase TiO_2 nanostructures with interconnected porous geometry onto FTO substrates. This process involved the deposition of presynthesized TiO_2 NP paste onto a Ti layer that had been sputter-deposited on the FTO substrate. This deposition was followed by a hydrothermal reaction in a 10 M NaOH aqueous solution at 130 °C for 2 h and then calcination at 500 °C for 30 min.[24] The results indicated that our approach provides a potential method for the deposition of porous TiO_2 nanostructures onto glass-based substrates, which is, importantly, favorable for AR-coating technology. However, the essential procedure of the TiO_2 NP paste preparation was very complicated; therefore, our aim was to simplify the preparation of the TiO_2 nanostructures through a one-step hydrothermal reaction, without predeposition of the TiO_2 NP paste. Herein, we present a one-step mild hydrothermal technique with a postannealing treatment for the preparation of 1D TiO_2 NWs on FTO substrates. The proposed process involves growing an anatase TiO_2 NW array with an oblique, highly porous, cross-linked nanostructure directly onto both sides of the FTO substrate through hydrothermally treating a FTO predeposited 100-nm-thick TiO_2 film under mild alkali conditions without damaging the FTO substrates. With such a unique structure, not only is the electrochromic performance of the TiO_2 NW-based device enhanced but also the optical transmittance of the device in the visible light range is improved. To the best of our knowledge, this is the first study to reveal that the intrinsic low-refractive index of this TiO_2 NW-array layer possesses excellent dual AR and electrochromic properties.

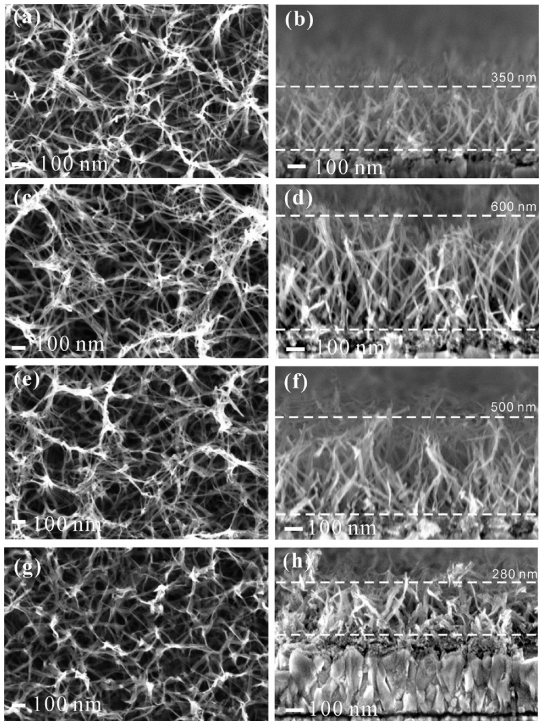

Figure 1. Top surface (left) and cross-sectional (right) FESEM images of the TiO_2 NW layers fabricated at a hydrothermal temperature of 80 °C for 1 h in (a, b) 2.5 M, (c, d) 5 M, (e, f) 7.5 M, and (g, h) 10 M NaOH aqueous solutions. The thickness of a TiO_2 NW layer is labeled on the cross-sectional images.

RESULTS AND DISCUSSION

Figure 1 shows the top surface and cross-sectional morphologies of the TiO_2 NW layers on FTO under mild alkali hydrothermal treatment. The treatment was carried out at 80 °C for 1 h in NaOH aqueous solutions at concentrations of 2.5, 5, 7.5, and 10 M, resulting in the fabrication of NW structures with thicknesses of approximately 350, 600, 500, and 280 nm, respectively. These results demonstrate that our simple one-step hydrothermal technique for the fabrication of 1D TiO_2 NWs can be successfully achieved under alkali conditions. The NaOH concentration governs the formation rate of the titanate species formed by the reaction of Ti with NaOH during the initial reaction in the further formation of TiO_2 nanomaterials.[19] Thus, increasing alkaline concentrations lead to accelerated dissolution of Ti, forming titanate species that in turn benefit the growth of TiO_2 NWs. However, as the concentration of NaOH increased to 7.5 and 10 M, somewhat short and rough surfaces of the TiO_2 NWs were observed (Figure 1e−h) as a result of the instability of the titanate species at the higher concentrations of NaOH solution. Also, the thickness of the TiO_2 NW layers increased with increasing NaOH concentration from 2.5 to 5 M, and then it decreased as the concentration of NaOH increased further (from 5 to 10 M). These results indicated that the alkali concentration strongly influences the growth of the TiO_2 nanostructure with 1D

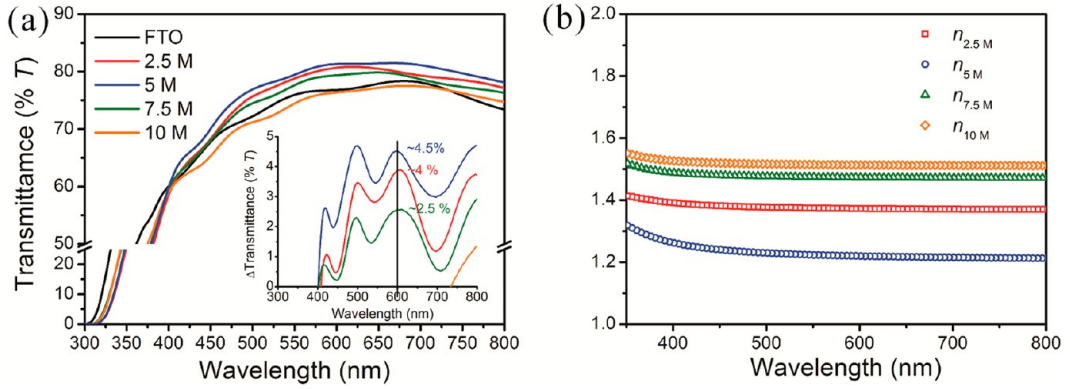

Figure 2. (a) Optical transmittance spectra of 2.5 M-, 5 M-, 7.5 M-, and 10 M-prepared TiO_2 NW FTO electrodes. Inset in part a: Difference in optical transmittance of FTO and each TiO_2 NW sample. (b) Refractive index curves for 2.5 M-, 5 M-, 7.5 M-, and 10 M-prepared TiO_2 NW FTO electrodes.

architectures, which is in accordance with our reported results.[24] Also, the well-defined anatase TiO_2 NW nanostructure was confirmed by characterizations using high-resolution transmission electron microscope (HRTEM), glancing-angle X-ray diffraction (XRD), and Raman spectrometry (Figure S1). The corresponding XRD pattern recorded from the TiO_2 NWs displayed diffraction 2θ values of approximately 25.1 and 48.5, which were assigned to the anatase TiO_2 (101) and anatase TiO_2 (200), respectively (JCPDS Card File No. 21-1272). The frequency of Raman bands showed a very strong band at 141 cm^{-1} and weak bands at 194, 394, 513, and 633 cm^{-1}. The three bands at 141, 194, and 633 cm^{-1} were assigned to the E_g modes, the band at 394 cm^{-1} to the B_{1g} mode, and the band at 515 cm^{-1} to the doublet of the A_{1g} and B_{1g} modes in anatase TiO_2. In addition, the typical HRTEM image together with its corresponding fast Fourier-transformed diffraction pattern data further showed that the TiO_2 NW was a single crystal with a lattice distance of approximately 0.35 nm, which is in excellent agreement with the *d*-spacing of (101) planes of anatase TiO_2 (Figure S1b).

All samples exhibited improved optical transmittance compared to that of bare FTO (Figure 2a). Also, it was obvious that with increasing NaOH concentration the optical transmittance at the wavelength of 600 nm initially increased and then decreased. The optical transmittance was enhanced by almost 4.5% for the TiO_2 NW FTO electrode prepared with 5 M NaOH (inset in Figure 2a). The increased optical transparency can be attributed to the intrinsic AR ability induced by the low-refractive-index TiO_2 NW layers. As shown in Figure 2b, the refractive index of the TiO_2 NW layers varied from 1.51 to 1.22 at a wavelength of 600 nm in NaOH concentrations of 2.5−10 M, which is less than that of dense anatase, 2.5,[25] because of their tendency to be porous as a result of randomly cross-linked TiO_2 NWs. The porosity of each TiO_2 NW electrode was determined by the following equation:[26,27]

$$\text{Porosity}\ (\%) = \left[1 - \frac{{n_f}^2 - 1}{{n_d}^2 - 1}\right] \times 100\% \qquad (1)$$

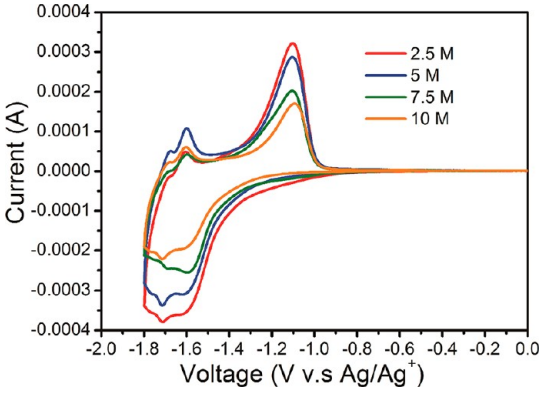

Figure 3. Cyclic voltammograms of 2.5 M-, 5 M-, 7.5 M-, and 10 M-prepared TiO_2 NW FTO electrodes at a scan rate of 5 mV/s.

where n_f and n_d are the refractive indices of TiO_2 NWs at the wavelength of 600 nm and anatase dense film (n_d = 2.5). The porosity for 2.5, 5, and 7.5 M TiO_2 NW layers was calculated as 83%, 91%, and 77%, respectively. Hence, the 5 M-prepared TiO_2 NW electrode possessed the highest transparency, which is attributed to the fact that it had the highest porosity degree and the lowest reflective value of 1.22. These results illustrated that the AR ability for promoting optical transparency of as-prepared TiO_2 NW electrodes is strongly dependent on their porosity degree, which in turn is determined by the degree of intersecting and crossing NWs. In contrast, the 10 M-prepared TiO_2 NW electrode exhibited 75% porosity and high refractive index (n_f = 1.51), which represented lower optical transmittance relative to the bare FTO glass due to the increased light scattering caused by irregular nanostructures on the surface.

With such promising results, we further investigated the electrochemical performance of TiO_2 NW electrodes in terms of other applications in electrochromic devices. Figure 3a shows the cyclic voltammograms of the as-prepared TiO_2 NW FTO substrates in 1 M $LiClO_4$ electrolyte, and two important features are noted. First, evident cathodic and anodic peaks appeared at approximately −1.6 and −1.1 V, respectively, for the

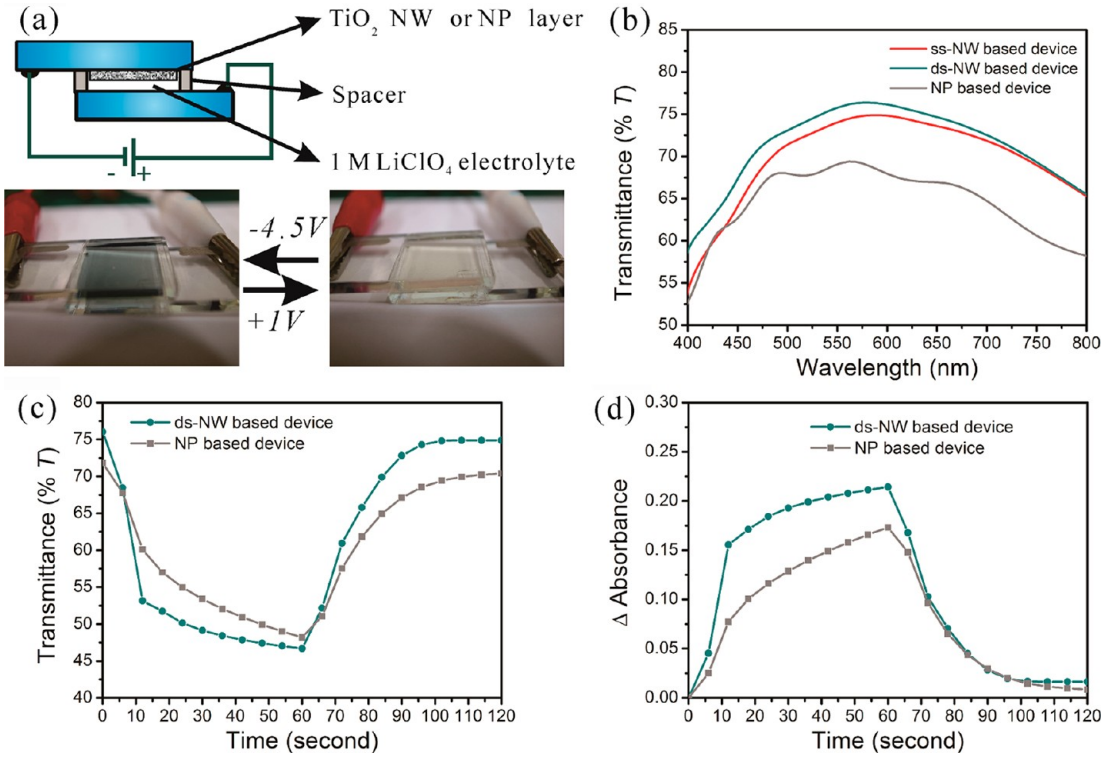

Figure 4. (a) Scheme of the electrochromic device and photos of the colored/bleached electrochromic devices after applying potentials of −4.5 and +1 V with respect to bare FTO. (b) Optical transmittance spectra for ss-NW-, ds-NW-, and NP-based FTO electrodes. (c) *In situ* UV−vis transmittance spectra at 600 nm of the electrochromic devices. (d) *In situ* UV−vis absorbance spectra at 600 nm collected by subtracting original absorbance of the electrochromic devices. The thickness of the TiO_2 NP layer is ~350 nm (Figure S5), similar to that of the 2.5 M-prepared TiO_2 NW layer.

Li^+ intercalation into and extraction from the TiO_2 framework. The corresponding reaction mechanism can be expressed by[28]

$$TiO_2 + xLi^+ + xe^- \leftrightarrows Li_xTiO_2$$

In addition, it should be noted that a weak redox pair occurred at approximately −1.7 V (cathodic) and −1.6 V (anodic), which was attributed to the characteristic peak of the Li^+ ion insertion into and release from the insufficiently calcined titanate, respectively (Figure S2). Second, electrodes prepared at lower alkali concentrations produced a higher current, resulting in better Li ion diffusion through the electrode. It is known that the higher the peak current, the larger the surface area of the electrode should be according to the Randles−Sevcik equation (eq 2), which could be beneficial for Li^+ intercalation and deintercalation.

$$i_p = (2.69 \times 10^5) n^{3/2} v^{1/2} D^{1/2} AC \qquad (2)$$

In eq 2, i_p is the peak current (A), n is the electron number involved in the reaction ($n = 1$ in this reaction), $v^{1/2}$ is the square root of the scan rate (V/s), A is the real active surface area of the working electrode (cm^2), and C is the concentration of Li^+ ions in the solution (mol/cm^3). It was found that the real active surface area of the TiO_2 NW FTO electrodes for the Li^+ intercalation process was larger in the following order of NaOH concentration as prepared in the hydrothermal process: 10 M < 7.5 M < 5 M < 2.5 M, which is in agreement with the results shown in Figure S3. These results indicated that the 2.5 M-prepared TiO_2 NW FTO electrode has the ability to support larger sites for Li ion intercalation and deintercalation, which is useful in electrochromic applications.

With such a low refractive index of 1.37, which is close to the theoretical refractive index of 1.39 for the most common AR-coating material magnesium fluoride (MgF_2),[29] and a high porosity of 85%, giving relatively high transparency and a high surface area, thereby profiting ion intercalation and deintercalation, it is anticipated that the 2.5 M-prepared TiO_2 NWs electrode will have the best utilization in transparent electrochromic smart windows. TiO_2-based multisandwich-type devices of glass/FTO/TiO_2/1 M $LiClO_4$ electrolyte/FTO/glass constructed from 2.5 M-prepared TiO_2 NWs (denoted as a ss-NW-based device) and TiO_2 NPs (denoted as a NP-based device) were used to study the electrochromic performance (Figure 4a). To further explore the feasibility of the 2.5 M-prepared TiO_2 NW layer in practical use, a similar device was constructed from the FTO substrate with a TiO_2 NW layer on both sides (denoted as a ds-NW-based device). The optical transmittance of the two NW-based devices exceeded 70% in the range 450−750 nm, covering the majority of the visible light region, whereas that of the NP-based

TABLE 1. Electrochromic Performance Data for ds-NW- and NP-Based Electrochromic Devices

	ΔOD	ΔQ (C cm^{-2})	CE (cm^2 C^{-1})
ds-NW-based device	0.21	0.015 14	13.87
NP-based device	0.16	0.012 99	12.32

device was below 70%. The optical transmittance of the ds-NW-based device increased by 8.2% and 1.3% at the wavelength of 600 nm relative to that of the NP-based device and the ss-NW-based device, respectively (Figure 4b). As a result, the double-sided AR coating of the ds-NW electrode, optimized for a glass substrate by enhancing the total optical transmittance in the visible region, has potential for use in high-transparency electrochromic devices. Its corresponding electrochromic performance measurement was carried out by measuring the optical transmittance and absorbance *in situ* at a wavelength of 600 nm in response to an applied potential of −4.5 V for 60 s as the coloring period and +1 V for another 60 s as the bleaching period through the devices (Figure 4c, d and Figure S4). The optical transmittance changing from the colored state (at 60 s) to the bleached state (at 120 s) for the ds-NW-based device (46.69% → 74.89%, ΔT = 28.20%) was higher than that of the NP-based device (48.20% → 70.43%, ΔT = 22.23%). This result indicated that the ds-NW-based device possessed a better color contrast, which makes it useful for electrochromic applications.

Electrochromic parameters involving the change in color density (ΔOD) and coloration efficiency (CE) of the ds-NW-based device were evaluated through the following equations:

$$\Delta OD = \log(T_b/T_c) \quad (3)$$

$$CE = \Delta OD/\Delta Q = [\log(T_b/T_c)]/\Delta Q \quad (4)$$

where ΔOD is the difference in optical density at a wavelength of 600 nm, which depends on the transmittances in the bleached (T_b) and colored (T_c) states. The value ΔQ (eq 5) is the inserted charge during the coloring period (0 s → 60 s) and is determined by integrating the current density passing through the device (Figure S6):

$$\Delta Q = \int_{t_1}^{t_2} j(t)\, dt \quad (5)$$

The calculated values of ΔOD, ΔQ, and the CE for the ds-NW-based device and NP-based device are listed in Table 1. The ds-NW-based device shows a higher color density of 0.21 and coloration efficiency of 13.87 cm^2 C^{-1} compared to the NP-based device (ΔOD = 0.16 and CE = 12.32 cm^2 C^{-1}), indicating its better electrochromic performance in terms of color contrast.

Fast color-switching time is another important factor for electrochromic applications. The color-switching

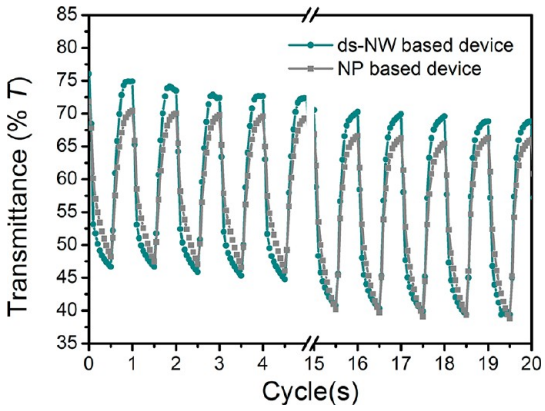

Figure 5. Electrochromic switching and optical transmittance change monitored at 600 nm for the cycling ability study of the ds-NW electrode- and NP-based device at an applied voltage of −4.5 V for 60 s and +1 V for 60 s for 20 cycles.

time was estimated as the time taken for the absorbance to change by two-thirds of the difference between the steady-state absorbance in the colored and bleached states (Figure 4d).[30] For the ds-NW-based device, the switching time was 11.3 s for coloration and 14.3 s for bleaching, which is significantly faster than the times for the NP-based device (23.7 s for coloration and 18.5 s for bleaching). This indicates that a fast electrochromic response can be achieved within the ds-NW-based device by rapidly diffusing Li^+ ions into and out of the TiO_2 NW layer, suggesting that the high porosity of the cross-linking NW structures plays an important role in ideal electrochromic materials.

Finally, stability can be a concern for the practical use of electrochromic materials. Therefore, an evaluation of the cycling durability for the ds-NW-based device and the NP-based device was performed (Figure 5). Good cycling efficiency and electrochemical stability can be observed in both devices, indicating the good cyclic durability of the TiO_2 materials. Noticeably, the cycling optical transmittance at a wavelength of 600 nm in the bleached state and the improved color contrast of the ds-NW-based device compared to that of the NP-based device can be observed. These findings clearly demonstrate that the anatase TiO_2 NW electrode possesses excellent electrochromic behavior, making it suitable for the development of high-transparency and high-color-contrast electrochromic smart windows.

CONCLUSIONS

To solve the long-standing problem of low transparency in conventional electrochromic devices, we developed a simple, one-step hydrothermal method for the fabrication of AR-coating films with good electrochromic properties. A highly transparent electrochromic device constructed from anatase TiO_2 NWs with an optical transmittance greater than 70% in the range 450−750 nm exhibited high color density (0.21), better coloration efficiency (13.87 cm^2 C^{-1}), and a faster

color-switching time (11.3 s for coloration and 14.3 s for bleaching) compared with TiO_2 NP-based devices. Moreover, we believe that our one-step alkali hydrothermal method will be amenable to processing new antireflective materials on common glass substrates, opening up possibilities for fabricating the devices for optical applications such as lens coatings, photocatalysis, and solar-energy conversion.

METHODS

Preparation of the TiO_2 NWs Layer(s) on FTO Glass. Titanium film with a thickness of approximately 100 nm was first deposited onto one or both sides of FTO glass (1.5 × 3 cm, 7 ohm/sq, TEC-7) to form a thin Ti-sputtered FTO glass. This was accomplished using a magnetic sputter instrument (K575X, Quorum Tech) equipped with a Ti target at a sputter rate of 3−5 Å/s. The thickness was controlled and monitored by a film thickness monitor controller. The Ti-sputtered FTO was subsequently treated under hydrothermal conditions in a Teflon vessel containing a 2.5 M NaOH (99%, Merck) aqueous solution encapsulated in a stainless-steel autoclave and then heated at 80 °C for 1 h. After the hydrothermal process, the substrate was rinsed several times with a 0.1 M HNO_3 (65%, Merck) aqueous solution and deionized water. The as-prepared product was further annealed in air at 500 °C for 1 h, which yielded the TiO_2 NW structure on FTO. The influence of the NaOH concentration (from 2.5 to 10 M in 2.5 M intervals) on the TiO_2 architectures was investigated in this study.

Fabrication of Multisandwich Electrochromic Devices. For the electrochromic contrast measurement, a simple electrochromic device based on a glass/FTO/TiO_2/1 M $LiClO_4$ electrolyte/FTO/glass multisandwich structure was prepared in three steps. In the first step, the as-prepared TiO_2−FTO substrate and counter FTO glass were attached with Surlyn 1702 hot-melt adhesive (Solaronix). In the second step, the electrolyte composed of $LiClO_4$ (1 M, 99% anhydrous, Aldrich) in propylene carbonate (97% anhydrous, Aldrich) was carefully injected, filling the space between the two substrates through a predrilled hole on the bare FTO using a vacuum filling process. Finally, the hole was covered by a thin glass slide with a hot-melt sealer and further sealed tightly with an iron solder. The electrochromic active area of the device was controlled at 1.69 cm^2.

Characterizations. The surface and cross-section morphologies of the as-prepared TiO_2 nanostructures were recorded by a Zeiss Ultraplus field-emission scanning electron microscope (FESEM). A JEM 2010 high-resolution transmission electron microscope operated at 200 kV was used to examine the morphology and lattice structure of the as-prepared TiO_2 NWs. The crystal structure was analyzed by Raman spectroscopy and glancing-angle X-ray powder diffraction, in which Raman spectra were obtained using a Raman microspectroscopic system (JOBIN-YVON T64000 Raman/PL spectrometer) with a diode semiconductor laser (λ = 532 nm) as a light source, and XRD patterns were recorded using the MAC M18XHF X-ray diffractometer equipped with Cu Kα radiation (λ = 1.5407 Å). The absorbance and transmittance spectra were obtained with a UV/vis/NIR spectrometer (Lambda 900, Perkin-Elmer). The reflectance and refractive indices measurements were carried out by using an n&k 1280 analyzer (n&k Technology), in which the refractive index n value was obtained through the Forouhi−Bloomer dispersion equation by fitting the transmittance and reflectance spectra of certain substrates.[31] The cyclic voltammograms of each as-prepared TiO_2 NW layer were recorded using a CH Instruments 660 electrochemical system with a standard three-electrode measurement, with aTiO_2 NW layer on FTO glass acting as the working electrode, a platinum plate serving as the counter electrode, and Ag/Ag^+ acting as the reference electrode. For the electrolyte, 1 M $LiClO_4$ dissolved in propylene carbonate was used. The potential of the $J-V$ measurement was controlled in the range 0 to −1.8 V at a potential sweep rate of 5 mV/s. The immersed area of the electrodes was controlled at 2.25 cm^2.

Conflict of Interest: The authors declare no competing financial interest.

Acknowledgment. We gratefully acknowledge the financial support of the National Science Council of Taiwan (NSC-101-2113-M-005-014-MY3; NSC-98-2113-M-005-004-MY3; NSC-98-2120-M-007-009) to support this work. We also thank Dr. Lih J. Chen at National Tsing Hua University, Taiwan, for providing technical assistance in HRTEM measurement.

Supporting Information Available: Morphology and structure characterizations of the as-prepared TiO_2 NWs; surface area measurement, electrochemical analysis, and current response measurement of NW-based TiO_2 electrode; electrochemical analysis of uncalcined titanate NWs; morphology characterization of TiO_2 NP layer. These materials are available free of charge *via* the Internet at http://pubs.acs.org.

REFERENCES AND NOTES

1. Granqvist, C. G. *Handbook of Inorganic Electrochromic Materials*; Elsevier: Amsterdam, 1995; pp 1−13.
2. Granqvist, C. G. Electrochromic Materials: Out of A Niche. *Nat. Mater.* **2006**, *5*, 89–90.
3. Jonsson, A.; Roos, A.; Jonson, E. K. The Effect on Transparency and Light Scattering of Dip Coated Antireflection Coatings on Window Glass and Electrochromic Foil. *Sol. Energy Mater. Sol. Cells* **2010**, *94*, 992–997.
4. Jonsson, A.; Roos, A. Visual and Energy Performance of Switchable Windows with Antireflection Coatings. *Sol. Energy* **2010**, *84*, 1370–1375.
5. Granqvist, C. G.; Green, S.; Jonson, E. K.; Marsal, R.; Niklasson, G. A.; Roos, A.; Topalian, Z.; Azens, A.; Georén, P.; Gustavsson, G.; *et al.* Electrochromic Foil-Based Devices: Optical Transmittance and Modulation Range, Effect of Ultraviolet Irradiation, and Quality Assessment by 1/f Current Noise. *Thin Solid Films* **2008**, *516*, 5921–5926.
6. Yonghong, Y.; Jiayu, Z.; Peifu, G.; Xu, L.; Jinfa, T. Electrochromism of Titanium Oxide Thin Films. *Thin Solid Films* **1997**, *298*, 197–199.
7. Shinde, P. S.; Deshmukh, H. P.; Mujawar, S. H.; Inamdar, A. I.; Patil, P. S. Spray Deposited Titanium Oxide Thin Films as Passive Counter Electrodes. *Electrochim. Acta* **2007**, *52*, 3114–3120.
8. Szlufcik, J.; Majewski, J.; Buczkowski, A.; Radojewski, J.; Jedral, L.; Radojewska, E. B. Screen-Printed Titanium Dioxide Anti-Reflection Coating for Silicon Solar Cells. *Sol. Energy Mater.* **1989**, *18*, 241–252.
9. Jin, P.; Xu, G.; Tazawa, M.; Yoshimura, K. Design, Formation and Characterization of A Novel Multifunctional Window with VO_2 and TiO_2 Coatings. *Appl. Phys. A: Mater. Sci. Process* **2003**, *77*, 455–459.
10. Chih-Hsiao, C.; Shunk, S. C.; Koren, U.; Chien, M.; Miller, B. I.; Dreyer, K. F.; Presby, H. M.; Ahrens, R. G. Semiconductor Optical Amplifier Array Coupled to Uncoated Flat-End Fibers with Integrated Beam Expanders and TiO_2 Antireflection Coatings. *IEEE J. Sel. Top. Quantum Electron.* **1998**, *3*, 1421–1428.
11. Heavens, O. S. *Optical Properties of Thin Solid Films*; Dover Publications Inc: New York, 1991; pp 209−210.
12. Synowicki, R. A. Spectroscopic Ellipsometry Characterization of Indium Tin Oxide Film Microstructure and Optical Constants. *Thin Solid Films* **1998**, *313−314*, 394–397.
13. Stjerna, B.; Olsson, E.; Granqvist, C. G. Optical and Electrical Properties of Radio Frequency Sputtered Tin Oxide Films Doped with Oxygen Vacancies, F, Sb, or Mo. *J. Appl. Phys.* **1994**, *76*, 3797–3817.
14. Xi, J. Q.; Schubert, M. F.; Kim, J. K.; Schubert, E. F.; Chen, M. F.; Lin, S. Y.; Liu, W.; Smart, J. A. Optical Thin-Film Materials

with Low Refractive Index for Broadband Elimination of Fresnel Reflection. *Nat. Photonics* **2007**, *1*, 176–179.
15. Gonzalez-Garcia, L.; Lozano, G.; Barranco, A.; Miguez, H.; Gonzalez-Elipe, A. R. TiO_2-SiO_2 One-Dimensional Photonic Crystals of Controlled Porosity by Glancing Angle Physical Vapour Deposition. *J. Mater. Chem.* **2010**, *20*, 6408–6412.
16. Hodgkinson, I.; Wu, Q. h.; Hazel, J. Empirical Equations for the Principal Refractive Indices and Column Angle of Obliquely Deposited Films of Tantalum Oxide, Titanium Oxide, and Zirconium Oxide. *Appl. Opt.* **1998**, *37*, 2653–2659.
17. Wang, S. M.; Xia, G. D.; He, H. B.; Yi, K.; Shao, J. D.; Fan, Z. X. Structural and Optical Properties of Nanostructured TiO_2 Thin Films Fabricated by Glancing Angle Deposition. *J. Alloy. Compd.* **2007**, *431*, 287–291.
18. Peng, X. S.; Chen, A. C. Large-Scale Synthesis and Characterization of TiO_2-Based Nanostructures on Ti Substrates. *Adv. Funct. Mater.* **2006**, *16*, 1355–1362.
19. Dong, W.; Zhang, T.; Epstein, J.; Cooney, L.; Wang, H.; Li, Y.; Jiang, Y.-B.; Cogbill, A.; Varadan, V.; Tian, Z. R. Multifunctional Nanowire Bioscaffolds on Titanium. *Chem. Mater.* **2007**, *19*, 4454–4459.
20. Liu, B.; Boercker, J. E.; Aydil, E. S. Oriented Single Crystalline Titanium Dioxide Nanowires. *Nanotechnology* **2008**, *19*, 505604.
21. Tian, Z. R. R.; Voigt, J. A.; Liu, J.; McKenzie, B.; Xu, H. F. Large Oriented Arrays and Continuous Films of TiO_2-Based Nanotubes. *J. Am. Chem. Soc.* **2003**, *125*, 12384–12385.
22. Chatterjee, S.; Bhattacharyya, S.; Khushalani, D.; Ayyub, P. Hydrothermally Synthesized Aligned Arrays of Self-Assembled Multiwalled Hydrogen Titanate Nanotubes. *Cryst. Growth Des.* **2010**, *10*, 1215–1220.
23. Huang, J.; Cao, Y.; Deng, Z.; Tong, H. Formation of Titanate Nanostructures under Different NaOH Concentration and Their Application in Wastewater Treatment. *J. Solid State Chem.* **2011**, *184*, 712–719.
24. Chen, J. Z.; Yen, Y. C.; Ko, W. Y.; Cheng, C. Y.; Lin, K. J. The Role of the Fabrication of Anatase-TiO_2 Chain-Networked Photoanodes. *Adv. Mater.* **2011**, *23*, 3970–3973.
25. Mor, G. K.; Varghese, O. K.; Paulose, M.; Grimes, C. A. Transparent Highly Ordered TiO_2 Nanotube Arrays *via* Anodization of Titanium Thin Films. *Adv. Funct. Mater.* **2005**, *15*, 1291–1296.
26. Yoldas, B. E.; Partlow, D. P. Formation of Broad Band Antireflective Coatings on Fused Silica for High Power Laser Applications. *Thin Solid Films* **1985**, *129*, 1–14.
27. Hu, L.; Yoko, T.; Kozuka, H.; Sakka, S. Effects of Solvent on Properties of Sol—Gel Derived TiO_2 Coating Films. *Thin Solid Films* **1992**, *219*, 18–23.
28. Hagfeldt, A.; Vlachopoulos, N.; Grätzel, M. Fast Electrochromic Switching with Nanocrystalline Oxide Semiconductor-Films. *J. Electrochem. Soc.* **1994**, *141*, L82–L84.
29. Yoldas, B. E. Investigations of Porous Oxides as An Antireflective Coating for Glass Surfaces. *Appl. Opt.* **1980**, *19*, 1425–1429.
30. Cummins, D.; Boschloo, G.; Ryan, M.; Corr, D.; Rao, S. N.; Fitzmaurice, D. Ultrafast Electrochromic Windows Based on Redox-Chromophore Modified Nanostructured Semiconducting and Conducting Films. *J. Phys. Chem. B* **2000**, *104*, 11449–11459.
31. Zhang, K.; Forouhi, A. R.; Bloomer, I. Accurate and Rapid Determination of Thickness, n and k Spectra, and Resistivity of Indium-Tin-Oxide Films. *J. Vac. Sci. Technol. A* **1999**, *17*, 1843–1847.